Received 4 September 2022; revised 17 October 2022; accepted 9 November 2022. Date of publication 16 November 2022; date of current version 30 November 2022.

Digital Object Identifier 10.1109/OJCOMS.2022.3222177

On the Quality of Service and Experience in IRS-NOMA Over $\kappa-\mu$ Generalized Fading Channels

ADEL ALQAHTANI [1] (Member, IEEE), AND EMAD ALSUSA [2] (Senior Member, IEEE)

[1]Department of Electrical Engineering, King Khalid University, Abha 61421, Saudi Arabia

[2]School of Electrical and Electronic Engineering, University of Manchester, M13 9PL Manchester, U.K.

CORRESPONDING AUTHOR: A. ALQAHTANI (e-mail: assaeeed@kku.edu.sa)

This work was supported in part by the European Union's Research and Innovation Program under the Marie Skłodowska-Curie Grant under Agreement 812991 "PAINLESS" within the Horizon 2020 Program.

ABSTRACT The quality of service (QoS) and quality of experience (QoE) metrics are vital performance indicators in cellular systems. This article presents an analytical study on indoor non-orthogonal multiple access (NOMA) systems empowered by intelligent reflecting surfaces (IRS) in generalized $\kappa-\mu$ fading channels. In particular, we consider the network's QoS through various performance metrics such as outage probability (OP), ergodic capacity (EC), average bit error rate (BER), and system throughput, for which we derive exact and asymptotic closed-form expressions. Furthermore, in contrast to measuring the conventional QoE of a user, we propose to apply the mean score opinion (MOS) factor, in which the objective technical criterion is mutated into a subjective user-recognized quality. To quantify this, a MOS-based QoE evaluation model is applied to an interactive Web browsing service. The results demonstrate the impact of IRS on the QoS and QoE of the indoor NOMA users, as well as the effect of manipulating the channel fading components, power allocation coefficients, and path loss factors. It will be shown that careful manipulation of such parameters, coupled with the use of IRS, produces spectacular improvements in system performance. Monte Carlo simulations are performed to corroborate the accuracy of the derived analytical results.

INDEX TERMS Non-orthogonal multiple access (NOMA), quality of service (QoS), quality of experience (QoE), and intelligent reflecting surface (IRS).

I. INTRODUCTION

DRIVEN by the dramatic demands for higher data rates and lower latency in 6G wireless networks, non-orthogonal multiple access (NOMA) and intelligent reflecting surfaces (IRS) have been considered potential techniques for future networks, [1], [2], [3]. In general, IRS is used to manipulate the mobile user's propagation environment to produce constructive multipath at the receiver, which in turn leads to tremendous enhancements in data throughput [4], [5]. Other advantages of IRS are low complexity, low power consumption, low infrastructure cost, and high spectral efficiency. Unlike traditional orthogonal multiple access (OMA) which serves onen individual user per resource block, the key concept of NOMA is to serve multiple users in each resource block. Therefore, NOMA is more suited for massive connectivity and low latency, due allowing dynamic spectrum sharing among users while achieving their quality of service (QoS) requirements [6], [7]. NOMA can also be combined with other wireless communication technologies, such as IRS, to actively manage the wireless communication environment to improve the reception reliability at a minimal cost [8]. As such, these two enabling technologies are complementary to each other, in the sense that NOMA enhances the spectral efficiency while IRS facilitates constructive propagation environments to maximize the received signal power [9], [10].

Several studies hae investigated the combination of NOMA with IRS. For example, Ding and Poor in [2] proposed a new design of NOMA transmission with IRS, which offers a low-cost antenna array involving a large number of IRS elements. This is done to ensure that multiple users can be served in each orthogonal spatial direction as compared to space division multiple access (SDMA). They also studied hardware impairments on the proposed

IRS-NOMA design, as well as the system performance under practical conditions. In [11], the authors integrated IRS with NOMA/OMA systems and proposed discrete phase shifts for the IRS reflection in order to decrease the transmit power for specific user rates. The results revealed that NOMA may be considered worse than TDMA for near-IRS users with symmetric rates. Thus, to overcome this problem, they proposed pairing the user with asymmetric rates. Moreover, IRS has been applied along with various wireless communication technologies in different scenarios due to its low power consumption property and channel manoeuvrability [12]. For example, the authors in [13], [14] studied the potential benefits of IRS on multiple UAVs and analyzed different performance metrics such as the symbol error rate (SER) and the average capacity. The practical assumption of phase error is considered in these studies on IRS, where the number of reflectors has a significant impact on the accuracy of phase estimation. Therefore, different theorems such as Sinusoidal Addition Theorem (SAT) and Central Limit Theorem (CLT) have been proposed to analyze a range of different numbers of IRS reflectors. Furthermore, asymptotic closed expressions were obtained for the probability of outage (OP) and the probability of the average symbol error of an IRS-assisted wireless power transfer (WPT) system in [12], demonstrating the strong performance improvement due to the IRS component. Furthermore, other research studies have recently been conducted on the combination of IRS and NOMA [15], [16], [17], [18]. Ding et al. in [15] investigated the impact of two types of IRS phase change (coherent phase shift and random discrete phase shift) on the performance of a NOMA network under various conditions. In [16], the authors analysed an IRS-assisted NOMA system and evaluated the OP and average channel capacity with exact closed-form expressions. Their findings indicate that the performance of IRS-supported NOMA networks is superior to that of an OMA system. Taking into account numerous antennas, Zhu et al. [17] evaluated an IRS-aided downlink multiple input single output (MISO) system by optimizing the beam formation vector and IRS phase change matrix simultaneously to decrease the transmission power. Furthermore, Fang et al. in [18], studied an IRS-assisted wireless power NOMA network where energy efficiency is optimized under the constraints of minimising the power consumption and maximising the sum data rate. In NOMA networks, different performance indicators have been investigated to measure the quality of service level (QoS), such as outage probability (OP), throughput, energy efficiency (EE), latency, etc. For example, Yahya et al. in [19] derived exact and asymptotic expressions for BER of NOMA systems under the assumption of a conventional fading channel with arbitrary number of phase-shift keying modulation orders. The results demonstrated the relationship between the power coefficients and the modulation order N, where the BER suffers increased inter-user interference as the modulation order increases. The authors determined the best optimal power allocation to minimize the system's average BER. Furthermore, ElHalawany et al. in [20] studied the performance of NOMA downlink and derived closed-form expressions of different QoS metrics including the ergodic capacity (EC), average BER, and OP, in which a shadowed fading model $\kappa - \mu$ is applied. Furthermore, Alqahtani et al. in [21] studied the QoS of multiple NOMA users by analysing OP, the average BER and the ergodic capacity (EC). The study showed that the interplay between the channel fading components, power allocation factors, and target data rates have significant impacts on QoS. However, users may experience different levels of quality of experience (QoE) even with the same throughput due to considerable variations in the type of applications and user preferences. The mean opinion score (MOS) is often used to assess the customer satisfaction with services such as video streaming, file download, and online browsing [22]. Sun et al. in [23] investigated the resource allocation problem for NOMA by applying the MOS to evaluate the user's QoE and maximize it. Furthermore, the authors in [24] proposed a QoE-assisted resource allocation algorithm for multi-cell-NOMA (MC-NOMA) network.

A. MOTIVATION AND CONTRIBUTION

In the above mentioned studies, it was assumed that the NOMA signal propagates through outdoor to outdoor channels. However, users could be indoors while being served by an outdoor BS. Therefore, the outdoor-to-indoor channel, or vice versa, is an important scenario that warrants investigation. As a consequence, the effectiveness of receiving reliable and strong transmission signals for indoor users gradually decreases due to restrictions inside the building and the path-loss. Therefore, we propose applying an IRS close to the BS to enhance the signal strength of indoor users as well as to improve the overall performance of the system. This approach effectively improves the performance of indoor users by acting as a virtual MIMO system to reduce the complexity while maintaining good energy efficiency as it lead to alleviating the limitations caused by the channel conditions of the indoor users. Unlike the progress published in [25], [26], where the proposed system model works under the assumption of orthogonal multiple access (OMA) system, the presented research in this paper focusses on the application of NOMA in future wireless networks. Beside, prior work in this area provides a limited analytical investigation on the combination of IRS and NOMA technologies, while this work attempts to provide a comprehensive investigation. In addition, and to the best of our knowledge, no analytical work has been carried out on the QoS and QoE performance of indoor IRS-NOMA systems over $\kappa - \mu$ fading channels. Thus, in this paper, our aim is to investigate QoS and QoE for multiple indoor IRS-assisted NOMA users over generalized fading channels. Although the open literature presents multiple studies on conventional outdoor NOMA integrated with IRS, these are not directly applicable for the case of indoor NOMA. Specifically, we investigate the proposed system model where the downlink

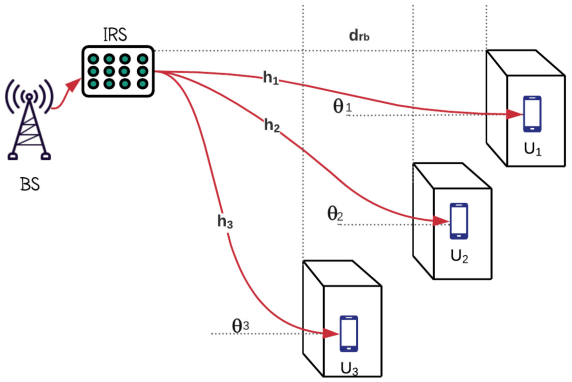

FIGURE 1. System model.

superimposed signal propagates via outdoor-to-indoor channels and we analyze the performance of the indoor NOMA users when considering the instantaneous channel gains of all the links. The contributions of this paper can thus be summarized as follows:

- Derive an expression for the SINR of multiple indoor users to find exact and asymptotic OP expressions over a generalised κ-μ fading channel when the user's data rate demand falls below certain QoS requirements.
- With the aid of the Fox H-function and the Meijer G-function, we derive exact and asymptotic analytical expressions for EC. In addition, closed-form expressions are obtained for the throughput of a three-indoor-user NOMA system under ideal assumptions.
- Evaluate the link performance and provide exact and asymptotic closed-form BER expressions for M-QAM modulation.
- Study the quality of experience of the indoor NOMA users when supported by IRS.
- Evaluate the performance of NOMA downlink signals propagating through outdoor-to-indoor channels, where they are ranked based on their instantaneous fading coefficients, and study the impact of the path loss characteristics on the indoor and outdoor users.
- Validate the accuracy of the derived expressions using Monte Carlo simulations.

The rest of this paper is organized as follows. Section II discusses the system model in this work. Section III provides the SINR analysis, OP, EC, BER, and throughput. The MOS based QoE evaluation model is presented in Section IV. Finally, the results of this work are discussed in Section V, while the conclusion is provided in Section VI.

II. SYSTEM MODEL

In this paper, an IRS-non-orthogonal multiple accessess (NOMAs) downlink system is considered, which consists of a single base station (BS), a single IRS panel equipped with N passive reflective elements and deployed close enough to the BS, and multiple legitimate indoor users. The main goal of applying such IRS model is to achieve high energy efficient transmission at low complexity setup. Assuming that

TABLE 1. The list of symbols and notations used in this paper.

Symbol	Definition
N	number of passive reflective elements
L_{fs}	loss of the free space path
d_{in}	distance between the building wall and indoor user
d_{rb}	distance between the UAV and the external building wall
L_{pc}	perpendicular loss
L_{pt}	parallel penetration loss
θ	grazing angle between BS and the external building wall
χ	loss of the indoor path
ϱ	number of internal walls
ϑ	loss of the internal walls
P_s	total transmitting power at BS
κ	channel fading parameter
μ	channel fading parameter
x_i	data symbol of user i
$\hbar$	channel coefficient
a_i	power allocation of user i
ρ	transmit signal to noise ratio
σ^2	noise variance
R_i	individual data rate of user i
$\mathcal{L}_1$	number of cycles required for the congestion window
$\mathcal{L}_2$	the amount of slow begin cycles required for web page size
ξ_1	experimental results of web browsing

the IRS has N reflectors with independent reflection phases, this leads to the realization of having an N-stream virtual MIMO system [25]. This approach was validated with the aid of a test-bed platform in [25], [26]. In spite of the setup's simplicity of the considered system model, the idea was to reserve the consumed energy used by multiple antennas and reduce the cost of the required infrastructure by employing an IRS close to the BS to communicate multiple outdoor to indoor users. In other words, the IRS is applied to enable energy-efficient and low-complexity application of MIMO transmitters [25]. Similar to the ones existing in the literature, many trusted research works such as [2] and [27] present straightforward system models to achieve effective methods of sustainable resources and discuss different analytical and optimized views. Therefore, this work attempts to study different performance metrics of pairing indoor users with outdoor BS through a passive IRS. However, the channel phase complexity caused by the IRS and its imperfections are out of the scope for this work, and the channel attenuation between the BS and the IRS is negligible [25], [26]. Hence, the considered IRS adjusts the phases of its reflector elements to cancel the channel phase terms to maximize the instantaneous signal-to-noise ratio (SNR), and the induced phase of each element is manipulated and optimized towards achieving this.

A. PATH LOSS MODEL

In this article, all active wireless channels are assumed to be independent and identically distributed (i.i.d.) and follow the generalised $\kappa-\mu$ fading model, where the channel state information (CSI) is assumed to be available at the BS. Furthermore, the legitimate received nodes can detect the NOMA signal over a single hop between the IRS and the indoor user, which is affected by the outdoor-to-indoor path loss. Therefore, the path loss model of the indoor NOMA environment, discussed in [28], is applied, and the total path loss for U_i can be calculated as

$$PL_i = L_{fs} + L_t + L_{in} \tag{1}$$

where L_{fs} represents the loss of the free space path, which can be given as $32.45 + 20\log_{10}((d_{rb} + d_i)) + 20\log_{10}(f)$, where d_i is the distance between the wall of the building and U_i, where $i \in \{1, 2, 3\}$, and d_{rb} is the distance between the IRS and the wall of the external building. Furthermore, L_t is known as the loss of the propagation transition path that involves the perpendicular loss L_{pc} and the parallel penetration loss L_{pt}. It can be given as

$$L_t = L_{pc} + L_{pt} \times (1 - \sin(\theta))^2 \tag{2}$$

where θ indicates the grazing angle between the IRS and the exterior wall of the building, given as $\theta = \cos^{-1}(d_{rb}/d_{out})$. Furthermore, the loss of the indoor propagation path, L_{in}, is obtained by the mean loss of the path selected from the interior side of the exterior wall, which can be calculated as

$$L_{in} = \max\left\{\varrho\vartheta, \chi(d_i - 2)(1 - \sin(\theta))^2\right\} \tag{3}$$

where χ is the parameter of loss of the indoor path, ϱ is the number of internal walls, and ϑ is the loss of the internal walls.

B. FADING CHANNEL DISTRIBUTION

$\kappa-\mu$ distribution involves small-scale variations in line of sight (LOS) signal scenarios. Hence, a fading $\kappa-\mu$ signal represents different clusters, $(\mu > 0)$, of multipath and scattered waves of similar power, as well as, arbitrary dominant power components established within each cluster. Therefore, the rate between these total components of the power is given as $(\kappa > 0)$. Furthermore, the appropriate probability density function (PDF) for the system model considered is given in the form of a sum of N i.i.d. $\kappa-\mu$ random variables (RV) as in [29].

$$f_\gamma(\gamma) = \frac{\mu(1+\kappa)^{\left(\frac{\mu+1}{2}\right)}\gamma^{\left(\frac{\mu-1}{2}\right)}}{\kappa^{\left(\frac{\mu-1}{2}\right)}\mathrm{e}^{(\mu\kappa)}\bar{\gamma}^{\left(\frac{\mu+1}{2}\right)}}\exp\left(\frac{-\mu(1+\kappa)\gamma}{\bar{\gamma}}\right) \times \mathrm{I}_{\mu-1}\left(2\mu\sqrt{\frac{\kappa(1+\kappa)\gamma}{\bar{\gamma}}}\right) \tag{4}$$

where the instantaneous SNR is illustrated as $\gamma \triangleq \rho|\hbar|^2 = \frac{\mathrm{P}}{\sigma^2}|\hbar|^2$. The notations of ρ, $\hbar$ and P are defined as the transmitted SNR, the channel frequency response, and the transmit power, respectively. In addition to that, the average SNR can be given as $\bar{\gamma} \triangleq \mathbb{E}[\gamma] = \Omega\frac{\mathrm{P}}{\sigma^2}$ with the expectation of $\mathbb{E}[.]$ and Ω defines the mean power of $\hbar$, i.e., $\mathbb{E}|\Omega| = [|\hbar|^2]$. $\mathrm{I}_v(.)$ is the modified Bessel function of the first kind. To achieve more tractable analysis, (4) cab be reduced to a further equivalent expression, particularly for $\mathrm{I}_v(.)$, by employing the series representation of $\mathrm{I}_v(.)$ represented in [30, eq. (8.445)]. Therefore, (4) is rewritten as

$$f_\gamma(\gamma) = \frac{1}{\mathrm{e}^{(N\mu\kappa)}}\sum_{c=0}^{\infty}\frac{(N\mu)^{2c+N\mu}\ \kappa^c\ (1+\kappa)^{c+N\mu}}{c!\ \Gamma(c+N\mu)\ \bar{\gamma}^{(c+N\mu)}} \times \gamma^{(c+N\mu-1)}\ \exp\left(-\frac{\mathrm{N}\mu(1+\kappa)\gamma}{\bar{\gamma}}\right). \tag{5}$$

Moreover, the related cumulative distribution function (CDF) of the sum of N fading channels of $\kappa-\mu$ is achieved by integrating the above PDF and is given in the form of the Fox H-function with the aid of [31, eq. (8.4.3.1) and (8.4.6.5)] and [32, eq. (6.2.8)]. Thus,

$$F_\gamma(\gamma) = \frac{1}{\mathrm{e}^{(N\mu\kappa)}}\sum_{c=0}^{\infty}\frac{(N\kappa\mu)^c}{c!\ \Gamma(c+N\mu)} \times \mathrm{H}_{1,2}^{1,1}\left[\frac{N\mu(1+\kappa)\gamma}{\bar{\gamma}}\middle|\begin{matrix}(1,1)\\(c+N\mu,1),(0,1)\end{matrix}\right]. \tag{6}$$

III. PERFORMANCE ANALYSIS

A. ANALYSIS OF SINR

The signal received by each user can be mathematically described as

$$y_i = \left(\sum_{n=1}^{N}\hbar_{i,n}e^{j\phi_{i,n}}\right) \times \underbrace{\left(\sum_i\sqrt{a_i\mathrm{P}_s}x_i\right)}_{x_{sc}} + n_i. \tag{7}$$

where P_s is the total transmission power in BS, and x_{sc} defines the superimposed signal, in which x_1, x_2 and x_3 represent the data symbols of U_1, U_2 and U_3, respectively. Furthermore, a_i represents the power allocation factor of the user i, and is given accordingly as $\sum_i^3 a_i = 1$ and $a_3 \le a_2 \le a_1$. $\hbar_{i,n} = \alpha_{i,n}e^{j\theta_{i,n}}$ illustrates the channel coefficient between the ith user and the nth passive reflector of the IRS, $n \in \{1, 2, \ldots, N\}$, where α_n and θ_n define its magnitude and phase, respectively. Hence, $\hbar_{1,n}$, $\hbar_{2,n}$ and $\hbar_{3,n}$ represents the channel coefficients of U_1, U_2 and U_3, respectively. We assume that each induced phase of the IRS passive reflector is given as $(\phi_{i,n} = -\theta_{i,n})$, which leads to the maximum SNR. Without loss of generality, the average channel gain between the BS and all indoor users are considered to be in ascending order as $|\sum_{n=1}^{N}\hbar_{1,n}|^2 \le |\sum_{n=1}^{N}\hbar_{2,n}|^2 \le |\sum_{n=1}^{N}\hbar_{3,n}|^2$, where we consider the effects of path loss and small-scale fading, which is modelled as the sum of N i.i.d. $\kappa-\mu$ random variables (RV) in this work. Furthermore, n_i indicates the additive white Gaussian noise (AWGN), where $n_i \sim \mathcal{CN}(0, \sigma_i^2)$. Thereafter, we assume that the noise powers of all users are identical in this work. Therefore, the signal-to-interference noise ratio (SINR) received at U_1 is

given below.

$$\gamma_{U_1}^{x_1} = \frac{a_1 \mathrm{P}_s \zeta_1}{a_2 \mathrm{P}_s \zeta_1 + a_3 \mathrm{P}_s \zeta_1 + \sigma^2} = \frac{a_1 \gamma_1}{a_2 \gamma_1 + a_3 \gamma_1 + 1}, \quad (8)$$

where $\zeta_1 = |\sum_{n=1}^{N} \hbar_{1,n}|^2$, $\rho = \frac{\mathrm{P}_s}{\sigma^2}$ and $\gamma_1 \triangleq \rho \zeta_1$, which is the instantaneous SNR at U_1.

In accordance with the NOMA principle, U_2 can detect U_1's signal and treat it as interference to be eliminated, and then decode its own signal while U_3's signal is treated as noise. This invokes the successive interference cancellation (SIC) principle. Subsequently, the SINR at U_2 is given to detect the symbols x_1 and x_2, respectively, as follows.

$$\gamma_{U_2}^{x_1 \to x_2} = \frac{a_1 \mathrm{P}_s \zeta_2}{a_2 \mathrm{P}_s \zeta_2 + a_3 \mathrm{P}_s \zeta_2 + \sigma^2} = \frac{a_1 \gamma_2}{a_2 \gamma_2 + a_3 \gamma_2 + 1} \quad (9)$$

$$\gamma_{U_2}^{x_2} = \frac{a_2 \mathrm{P}_s \zeta_2}{a_3 \mathrm{P}_s \zeta_2 + \sigma^2} = \frac{a_2 \gamma_2}{a_3 \gamma_2 + 1}, \quad (10)$$

where $\zeta_2 = |\sum_{n=1}^{N} \hbar_{2,n}|^2$ and $\gamma_2 \triangleq \rho \zeta_2$, which is the instantaneous SNR at U_2. Similarly, U_3 treats the signals of other users as interference and applies SIC to decode and eliminate them to obtain its own signal. Therefore, the SINR at U_3 to detect the symbols x_1, x_2, and x_3 are given, respectively, as follows.

$$\gamma_{U_3}^{x_1 \to x_2} = \frac{a_1 \mathrm{P}_s \zeta_3}{a_2 \mathrm{P}_s \zeta_3 + a_3 \mathrm{P}_s \zeta_3 + \sigma^2} = \frac{a_1 \gamma_3}{a_2 \gamma_3 + a_3 \gamma_3 + 1} \quad (11)$$

$$\gamma_{U_3}^{x_2 \to x_3} = \frac{a_2 \mathrm{P}_s \zeta_3}{a_3 \mathrm{P}_s \zeta_3 + \sigma^2} = \frac{a_2 \gamma_3}{a_3 \gamma_3 + 1} \quad (12)$$

$$\gamma_{U_3}^{x_3} = \frac{a_3 \mathrm{P}_s \zeta_3}{\sigma^2} = a_3 \gamma_3, \quad (13)$$

where $\zeta_3 = |\sum_{n=1}^{N} \hbar_{3,n}|^2$ and $\gamma_3 \triangleq \rho \zeta_3$, which is the instantaneous SNR at U_3.

B. OUTAGE PERFORMANCE (OP)

Essentially, the OP analysis involves the scenario in which the individual user's data rate must satisfy a certain quality of service (QoS). Therefore, the outage event of U_1 appears when its SINR or data rate is less than a threshold or a predefined data rate, and it can be expressed as

$$\mathrm{P}_{U_1}^{out} = \underbrace{\mathrm{P}_r\left(\gamma_{U_1}^{x_1} < \gamma_{th_1}\right)}_{E_{11}}, \quad (14)$$

where $\gamma_{th_1} = 2^{\mathrm{R}_1} - 1$, and R_1 is the target data rate of U_1. Now, submitting (8) into E_{11} yields the following expression.

$$E_{11} = \mathrm{P}_r\left(\gamma_1 < \frac{\gamma_{th_1}}{\left(a_1 - a_2\gamma_{th_1} - a_3\gamma_{th_1}\right)} \triangleq \varepsilon_1\right) = F_\gamma(\varepsilon_1). \quad (15)$$

Now, (6) is substituted into (15), and then the result is re-substituted into (14), resulting in

$$\mathrm{P}_{U_1}^{out} = 1 - \left(1 - \frac{1}{\mathrm{e}^{(N\mu\kappa)}} \sum_{c=0}^{\infty} \frac{(N\kappa\mu)^c}{c!\ \Gamma(c+N\mu)} \times \mathrm{H}_{1,2}^{1,1}\left[\frac{N\mu(1+\kappa)\varepsilon_1}{\bar{\gamma}_1}\middle| \begin{matrix}(1,1)\\(c+N\mu,1),(0,1)\end{matrix}\right]\right). \quad (16)$$

Similarly, U_2 can be out of service if its SINR or U_1's SINR are below certain thresholds. In other words, outage events of U_2 are considered when the U_1' s signal is incorrectly decoded at U_2 during the SIC process or if its own signal (x_2) is also improperly decoded. As a result, the OP of U_2 can be obtained as follows.

$$\mathrm{P}_{U_2}^{out} = 1 - \mathrm{P}_r\left(\gamma_{U_2}^{x_1 \to x_2} > \gamma_{th_1}, \gamma_{U_2}^{x_2} > \gamma_{th_2}\right) = 1 - \left[\left(1 - \mathrm{P}_r\left(\gamma_{U_2}^{x_1 \to x_2} < \gamma_{th_1}\right)\right)\left(1 - \mathrm{P}_r\left(\gamma_{U_2}^{x_2} < \gamma_{th_2}\right)\right)\right]. \quad (17)$$

By substituting (10) and (11) into (17), and following the same procedures as (14)-(16), the OP of U_2 can be given in closed form as follows

$$\mathrm{P}_{U_2}^{out} = 1 - \prod_{i=1}^{2}\left(1 - \frac{1}{\mathrm{e}^{(N\mu\kappa)}} \sum_{c=0}^{\infty} \frac{(N\kappa\mu)^c}{c!\ \Gamma(c+N\mu)} \mathrm{H}_{1,2}^{1,1}\left[\frac{N\mu(1+\kappa)\varepsilon_{2,i}}{\bar{\gamma}_2}\middle| \begin{matrix}(1,1)\\(c+N\mu,1),(0,1)\end{matrix}\right]\right). \quad (18)$$

where $\varepsilon_{2,1} = \varepsilon_1$ and $\varepsilon_{2,2} = \frac{\gamma_{th_2}}{(a2 - a3\gamma_{th_2})}$.

In a similar fashion, U_3 can experience an outage if its own SINR or U_1's SINR or U_2's SINR are below certain thresholds. Consequently, the outage events of U_3 are presented when the U_1's or U_2's signals are imprecisely decoded by U_3 during the SIC process or if its own signal (x_3) is also incorrectly decoded. Thereafter, the OP of U_3 can be illustrated as follows.

$$\mathrm{P}_{U_3}^{out} = 1 - \mathrm{P}_r\left(\gamma_{U_3}^{x_1 \to x_2} > \gamma_{th_1}, \gamma_{U_3}^{x_2 \to x_3} > \gamma_{th_2}, \gamma_{U_3}^{x_3} > \gamma_{th_3}\right) = 1 - \left[\left(1 - \mathrm{P}_r\left(\gamma_{U_3}^{x_1 \to x_2} < \gamma_{th_1}\right)\right) \left(1 - \mathrm{P}_r\left(\gamma_{U_3}^{x_2 \to x_3} < \gamma_{th_2}\right)\right)\left(1 - \mathrm{P}_r\left(\gamma_{U_3}^{x_3} < \gamma_{th_3}\right)\right)\right]. \quad (19)$$

We follow the same previous steps to find the final format of OP of U_3 as follows.

$$\mathrm{P}_{U_3}^{out} = 1 - \prod_{i=1}^{3}\left(1 - \frac{1}{\mathrm{e}^{(N\mu\kappa)}} \sum_{c=0}^{\infty} \frac{(N\kappa\mu)^c}{c!\ \Gamma(c+N\mu)} \times \mathrm{H}_{1,1}^{1,2}\left[\frac{N\mu(1+\kappa)\varepsilon_{3,i}}{\bar{\gamma}_3}\middle| \begin{matrix}(1,1)\\(c+N\mu,1),(0,1)\end{matrix}\right]\right), \quad (20)$$

where $\varepsilon_{3,1} = \varepsilon_1$, $\varepsilon_{3,2} = \varepsilon_{2,2}$ and $\varepsilon_{3,3} = \frac{\gamma_{th_3}}{a3}$.

To seek further insight, we aim to investigate the asymptotic OP at high SNR, i.e., ($\bar{\gamma} \to \infty$). Therefore, we use the following asymptotic expression of the Fox H function given in [33] as follows.

$$\lim_{z \to 0} \mathrm{H}_{p,q}^{m,n} \cong \sum_{j=1}^{m}\left[h_i z^{\frac{b_j}{\beta_j}} + \mathcal{O}\left(z\frac{b_j+1}{\beta_j}\right)\right], \quad (24)$$

where $\mathcal{O}$ indicates the high order and h_j is defined as follows.

$$h_j = \frac{\prod_{i=1,i\neq j}^{m} \Gamma\left(b_i - \frac{b_j\beta_i}{\beta_j}\right) \prod_{i=1}^{n} \Gamma\left(1 - a_i + \frac{b_j a_i}{\beta_j}\right)}{\beta_j \prod_{i=1+n}^{p} \Gamma\left(a_i - \frac{b_j a_i}{\beta_j}\right) \prod_{i=1+m}^{q} \Gamma\left(1 - b_i + \frac{b_j\beta_i}{\beta_j}\right)}. \tag{25}$$

Now, the asymptotic OP expressions of all users are achieved by applying the above identity to (16), (18) and (20), and they are stated at the bottom of the next page.

C. THROUGHPUT ANALYSIS

The system throughput of each user in a delay-limited transmission mode can be evaluated by its OP or ergodic capacity. Therefore, the corresponding outage throughput of a two-user NOMA system is given as follows.

$$\mathrm{T}_i^{\mathrm{OP}} = \left(1 - \mathrm{P}_i^{out}\right) \times \mathrm{R}_i, \tag{26}$$

where R_i is the individual data rate of user i. Therefore, we substitute (16), (18) and (20) in (26), separately, to obtain the throughput of all legitimate users.

D. AVERAGE BIT ERROR RATE (BER)

It is common practise to assess the quality of communication links in the presence of fading by characterising the conditional function of (BER) over the probability density function of the instantaneous signal-to-noise ratio (SNR) of the fading channel. For a wide range of wireless systems, the expressions for BER can be given as in [34] as follows.

$$\bar{P}_l^e = \int_0^{\infty} P_l^e \, f_{\gamma_l}(\gamma) d\gamma, \tag{27}$$

where $l \in \{1, 2, 3\}$. In this subsection, we consider three different indoor NOMA users with similar modulation orders using QAM, i.e., $M_l = 4 \ \forall l$, $l \in 1, 2, 3$, and the average BER performance is investigated over κ-μ fading model. The conditional BER (P_l^e) of the three users can be given, respectively, in terms of Q(.) as in [21].

$$P_1^e = \frac{1}{4} \sum_{i=1}^{4} \mathrm{Q}\left(\sqrt{\lambda_{3,i}\gamma_1}\right) \tag{28}$$

$$P_2^e = \frac{1}{4} \sum_{i=5}^{14} c_i \times \mathrm{Q}\left(\sqrt{\lambda_{3,i}\gamma_1}\right) \tag{29}$$

$$P_3^e = \frac{1}{4} \sum_{i=15}^{33} d_i \times \mathrm{Q}\left(\sqrt{\lambda_{3,i}\gamma_1}\right) \tag{30}$$

where $d_i = [4, -2, 2, 1, -1, 1, -2, 2, -2, 1, 1, -1, 1, -1, 2, -1, -1, 1, -1]$, $c_i = [1, -1, 2, 1, -1, 2, 1, -1, 1, -1]$, and $\gamma_{3,i}$ can be found in [21, Table 1]. Now, we submit (28) in (27). Thus, the following expression is obtained.

$$P_1^e = \frac{1}{4} \sum_{i=1}^{4} \Bigg[\mathcal{D}_1 \int_0^{\infty} {\gamma_1}^{c+N\mu-1} \exp\left(-\frac{N\mu(1+\kappa)\gamma}{\bar{\gamma}}\right) \mathrm{Q}\left(\sqrt{\lambda_{3,i}\gamma_1}\right) f_{\gamma_l}(\gamma) d\gamma \Bigg]. \tag{31}$$

where $\mathcal{D}_1 = \frac{1}{\mathrm{e}^{(N\mu\kappa)}} \sum_{c=0}^{\infty} \frac{(N\mu)^{2c+N\mu} \kappa^c (1+\kappa)^{c+N\mu}}{c! \ \Gamma(c+N\mu) \bar{\gamma}_1^{(c+N\mu)}}$. With the aid of [31, eq. (8.4.3.1), (8.4.14.2), and (8.4.16.1)], [32, eq. (6.2.8)], and the identity of $\mathrm{Q}(x) = \frac{1}{2}\mathrm{erfc}(\frac{x}{\sqrt{2}})$, the integral in (28) can be evaluated as follows.

$$I_1 = \frac{1}{\sqrt{\pi}} \int_0^{\infty} {\gamma_1}^{(c+N\mu-1)} \ \mathrm{G}_{0,1}^{1,0}\left[\frac{N\mu(1+\kappa)\gamma}{\bar{\gamma}} \middle| \begin{matrix} - \\ 0 \end{matrix}\right] \times \mathrm{G}_{1,2}^{2,0}\left[\frac{\lambda_{3,i}\gamma_1}{2} \middle| \begin{matrix} 1 \\ 0, \frac{1}{2} \end{matrix}\right] d\gamma_1. \tag{32}$$

The integral above in (32) can be solved by using the Mellin transform of the two-fox H function, given in [35], as

$$I_1 = \frac{1}{\sqrt{\pi}} \left(\frac{\lambda_{3,i}}{2}\right)^{-(c+N\mu)} \tag{33}$$

$$\times \mathrm{H}_{2,2}^{1,2}\left[\frac{N\mu(1+\kappa)}{\bar{\gamma}_1}\delta^{-1} \middle| \begin{matrix} (1-c-N\mu, 1) & \left(\frac{1}{2}-c-N\mu, 1\right) \\ (0, 1) & (-c-N\mu, 1) \end{matrix}\right], \tag{34}$$

where $\delta = (\frac{\lambda_{3,i}}{2})$. Substituting (33) into (31), the average BER of U_1 is given at the bottom of the page. Likewise, we follow the same procedures as applied for U_1 to obtain the average BER of the remaining users. As a result, (36) and (37), given at the bottom of the page, express the average BER of U_2 and U_3, respectively.

At high SNR, the asymptotic expression of the average BER can be achieved for all users by using the identity of (20) in (35)-(37). Therefore, the closed asymptotic expressions of all users are given at the bottom of the next page in (38)-(40).

$$\mathrm{P}_{U_1}^{out}(\infty) = 1 - \left(1 - \frac{1}{\mathrm{e}^{(N\mu\kappa)}} \sum_{c=0}^{\infty} \frac{(N\kappa\mu)^c}{c! \ \Gamma(1+c+N\mu)} \times \left(\frac{N\mu(1+\kappa)\varepsilon_1}{\bar{\gamma}_1}\right)^{c+N\mu}\right). \tag{21}$$

$$\mathrm{P}_{U_2}^{out}(\infty) = 1 - \prod_{i=1}^{2}\left(1 - \frac{1}{\mathrm{e}^{(N\mu\kappa)}} \sum_{c=0}^{\infty} \frac{(N\kappa\mu)^c}{c! \ \Gamma(1+c+N\mu)} \times \left(\frac{N\mu(1+\kappa)\varepsilon_{2,i}}{\bar{\gamma}_2}\right)^{c+N\mu}\right). \tag{22}$$

$$\mathrm{P}_{U_3}^{out}(\infty) = 1 - \prod_{i=1}^{3}\left(1 - \frac{1}{\mathrm{e}^{(N\mu\kappa)}} \sum_{c=0}^{\infty} \frac{(N\kappa\mu)^c}{c! \ \Gamma(1+c+N\mu)} \times \left(\frac{N\mu(1+\kappa)\varepsilon_{3,i}}{\bar{\gamma}_3}\right)^{c+N\mu}\right). \tag{23}$$

TABLE 2. Definitions for the symbols used in formulations.

Symbol	Definition	Symbol	Definition	Symbol	Definition
$\lambda_{3,1},\lambda_{3,6},\lambda_{3,33}$	$A_1+A_2+A_3$	$\lambda_{3,2},\lambda_{3,11},\lambda_{3,30}$	$A_1-A_2+A_3$	$\lambda_{3,3},\lambda_{3,14},\lambda_{3,24}$	$A_1+A_2-A_3$
$\lambda_{3,4},\lambda_{3,8},\lambda_{3,18}$	$A_1-A_2-A_3$	$\lambda_{3,5},\lambda_{3,31}$	$2A_1+A_2+A_3$	$\lambda_{3,7}$	A_2+A_3
$\lambda_{3,9},\lambda_{3,20}$	$2A_1-A_2-A_3$	$\lambda_{3,10},\lambda_{3,22}$	A_2-A_3	$\lambda_{3,12},\lambda_{3,28}$	$2A_1-A_2+A_3$
$\lambda_{3,13},\lambda_{3,25}$	$2A_1+A_2-A_3$	$\lambda_{3,15}$	A_3	$\lambda_{3,16}$	A_2+A_3
$\lambda_{3,17}$	$2A_2+A_3$	$\lambda_{3,19}$	$2A_1-2A_2-A_3$	$\lambda_{3,21}$	$2A_1-A_3$
$\lambda_{3,23}$	$2A_2-A_3$	$\lambda_{3,26}$	$2A_1+2A_2-A_3$	$\lambda_{3,29}$	$2A_1+A_3$
$\lambda_{3,32}$	$2A_1+2A_2+A_3$	$\lambda_{3,27}$	$2A_1-2A_2+A_3$		
$A_1=\sqrt{a_1},\ A_2=\sqrt{a_2},\ A_3=\sqrt{a_3}$					

E. AVERAGE CHANNEL CAPACITY

The Shannon channel fading capacity, which is also known as the ergodic capacity in (bits/s/Hz), is defined in [34] as

$$\bar{C}_l = \mathrm{BW}\int_0^{\infty}\log_2(1+\gamma_l)f_{\gamma_l}(\gamma_l)d\gamma_l. \tag{41}$$

where BW indicates the total bandwidth, and $l\in\{1,2,3\}$.

For the case of $l=1$, we substitute (8) in (41) and recall the identity of $\log_e(x)=\ln(x)/\ln(e)$. Thus, after some algebraic manipulations, we can obtain the following expression.

$$\bar{C}_1 = \frac{\mathrm{BW}}{\ln(2)}\Bigg[\underbrace{\int_0^{\infty}\ln(1+\gamma_1)f_{\gamma_1}(\gamma_1)d\gamma_1}_{\mathcal{I}_1} - \underbrace{\int_0^{\infty}\ln(1+\Psi\gamma_1)f_{\gamma_1}(\gamma_1)d\gamma_1}_{\mathcal{I}_2}\Bigg], \tag{42}$$

where $\Psi=(1-a_1)$. Substituting (5) and (8) into the integral of $\mathcal{I}_1$, and applying further manipulations, the following is obtained.

$$\mathcal{I}_1 = \int_0^{\infty}\gamma_1^{c+N\mu-1}\exp\left(-\frac{N\mu(1+\kappa)\gamma_1}{\bar{\gamma}_1}\right) \times\ln(1+\gamma_1)d\gamma_1\times\mathcal{D}_1, \tag{43}$$

where $\mathcal{D}_1$ is defined in (31). The above integral can be expressed in a compact form by rewriting exponential and logarithmic functions in their alternative Meijer G function formats defined in [31, eq. (8.4.3.1) and (8.4.6.5)]. Thus,

$$\mathcal{I}_1 = \mathcal{D}_1\times\int_0^{\infty}\gamma_1^{(C+N\mu-1)}\,\mathrm{G}_{0,1}^{1,0}\left[\frac{\gamma_1 N\mu(1+\kappa)}{\bar{\gamma}_1}\middle|\begin{matrix}-\\0\end{matrix}\right] \times\mathrm{G}_{2,2}^{1,2}\left[\gamma_1\middle|\begin{matrix}1,1\\1,0\end{matrix}\right]d\gamma_1. \tag{44}$$

To solve the above integral in a closed form, we aim to perform the identity in [36]. Thus, the following expression is obtained.

$$\mathcal{I}_1 = \mathrm{G}_{3,2}^{1,3}\left[\left(\frac{N\mu(1+\kappa)}{\bar{\gamma}_1}\right)^{-1}\middle|\begin{matrix}1,1,1-(c+N\mu)\\1,0\end{matrix}\right] \times\mathcal{D}_1\Upsilon_1, \tag{45}$$

$$\bar{P}_1^e = \frac{1}{4}\sum_{i=1}^{4}\left(\frac{1}{\sqrt{\pi}}\mathcal{D}_1(\delta)^{-(c+N\mu)}\times\mathrm{H}_{2,2}^{1,2}\left[\frac{N\mu(1+\kappa)}{\bar{\gamma}_1}(\delta)^{-1}\middle|\begin{matrix}(1-c-N\mu,1)&\left(\frac{1}{2}-c-N\mu,1\right)\\(0,1)&(-c-N\mu,1)\end{matrix}\right]\right). \tag{35}$$

$$\bar{P}_2^e = \frac{1}{4}\sum_{i=5}^{14}\left(\frac{1}{\sqrt{\pi}}\mathcal{D}_2\ c_i(\delta)^{-(c+N\mu)}\times\mathrm{H}_{2,2}^{1,2}\left[\frac{N\mu(1+\kappa)}{\bar{\gamma}_2}(\delta)^{-1}\middle|\begin{matrix}(1-c-N\mu,1)&\left(\frac{1}{2}-c-N\mu,1\right)\\(0,1)&(-c-N\mu,1)\end{matrix}\right]\right). \tag{36}$$

$$\bar{P}_3^e = \frac{1}{4}\sum_{i=15}^{33}\left(\frac{1}{\sqrt{\pi}}\mathcal{D}_3\ d_i(\delta)^{-(c+N\mu)}\times\mathrm{H}_{2,2}^{1,2}\left[\frac{N\mu(1+\kappa)}{\bar{\gamma}_3}(\delta)^{-1}\middle|\begin{matrix}(1-c-N\mu,1)&\left(\frac{1}{2}-c-N\mu,1\right)\\(0,1)&(-c-N\mu,1)\end{matrix}\right]\right). \tag{37}$$

$$\bar{P}_1^{e(\infty)} = \frac{1}{4}\sum_{i=1}^{4}\left[\frac{1}{\sqrt{\pi}}\mathcal{D}_1(\delta)^{-(c+N\mu)}\times\frac{\Gamma(c+N\mu)\Gamma\left(\frac{1}{2}+c+N\mu\right)}{\Gamma(1+c+N\mu)}\right]. \tag{38}$$

$$\bar{P}_2^{e(\infty)} = \frac{1}{4}\sum_{i=5}^{14}\left(\frac{1}{\sqrt{\pi}}\mathcal{D}_2\ c_i(\delta)^{-(c+N\mu)}\times\frac{\Gamma(c+N\mu)\Gamma\left(\frac{1}{2}+c+N\mu\right)}{\Gamma(1+c+N\mu)}\right]. \tag{39}$$

$$\bar{P}_3^{e(\infty)} = \frac{1}{4}\sum_{i=15}^{33}\left(\frac{1}{\sqrt{\pi}}\mathcal{D}_3\ d_i(\delta)^{-(c+N\mu)}\times\frac{\Gamma(c+N\mu)\Gamma\left(\frac{1}{2}+c+N\mu\right)}{\Gamma(1+c+N\mu)}\right]. \tag{40}$$

where $\Upsilon_1 = (\frac{N\mu(1+\kappa)}{\bar{\gamma}_1})^{-(c+N\mu)}$. Now, we follow the same derivation from (42)-(44) to solve the integral of $\mathcal{I}_2$. Thus, the following result is achieved.

$$\mathcal{I}_2 = \mathrm{G}_{3,2}^{1,3}\left[\Psi\left(\frac{N\mu(1+\kappa)}{\bar{\gamma}_1}\right)^{-1}\middle|\begin{matrix}1,1,1-(c+N\mu)\\1,0\end{matrix}\right] \times \mathcal{D}_1\Upsilon_1. \tag{46}$$

Now, we submit the results obtained in (45) and (46) to (42). Thus, the final exact expression of the average channel capacity of U_1 is expressed in (47) at the bottom of the page. To reach the remaining achievable average capacity of U_2 and U_3, a similar derivation approach from (42)-(47) is applied for both users. Therefore, (48) and (49), shown at the bottom of the page, represent closed-form expressions of ergodic capacity for U_2 and U_3, respectively. Therefore, $\Upsilon_l = (\frac{N\mu(1+\kappa)}{\bar{\gamma}_l})^{-(c+N\mu)}$ and $\mathcal{D}_l = \frac{1}{\mathrm{e}^{(N\mu\kappa)}}\sum_{c=0}^{\infty}\frac{N(\mu)^{2c+N\mu}\kappa^c(1+\kappa)^{c+N\mu}}{c!\ \Gamma(c+N\mu)(\bar{\gamma}_l)^{(c+N\mu)}}$, where $l \in \{1,2,3\}$.

F. CONVERGENCE OF THE INFINITE SERIES

An alternative form of (4) has been obtained in (5) y applying a series representation for the Bessel function of the first kind $\mathrm{I}_v(.)$ represented in [30, eq. (8.445)]; that is

$$\mathrm{I}_v(x) = \sum_{c=0}^{\infty}\frac{1}{c!\ \Gamma(c+v+1)}\left(\frac{x}{2}\right)^{2m+v} \tag{50}$$

As a result, the infinite series form offered in (16) can be shortened to a few terms and used to approximate the OP expression. Thus, (16) can be rewritten as follow.

$$\mathrm{P}_{U_1}^{out} \geq 1 - \left(1 - \frac{1}{\mathrm{e}^{(N\mu\kappa)}}\sum_{c=0}^{\mathrm{T}}\frac{(N\kappa\mu)^c}{c!\ \Gamma(c+N\mu)} \times \mathrm{H}_{1,2}^{1,1}\left[\frac{N\mu(1+\kappa)\varepsilon_1}{\bar{\gamma}_1}\middle|\begin{matrix}(1,1)\\(c+N\mu,1),(0,1)\end{matrix}\right]\right). \tag{51}$$

Depending on how severe the fading is, T, the number of terms in each series, should be changed. As can be noticed in Fig. 2, When the channel exhibits extreme fading, i.e., $(\kappa = 0, \mu = 2)$, a limited number of terms is necessary to produce a precise approximation. In this scenario, a total of $\mathrm{T} = 5$ terms are employed. However, in a less severe fading situation $(\kappa = 4.5, \mu = 4.5)$, as shown in Fig. 8, additional terms are essential for improved accuracy (a total of $\mathrm{T} = 25$ terms are utilized in this case). One notable feature of the suggested approach is that it converges to the exact OP for large SNR, even though only a few terms in the series are used. This approach is intended to be applied to any remaining exact and asymptotic expressions that incorporate a series representation in this work.

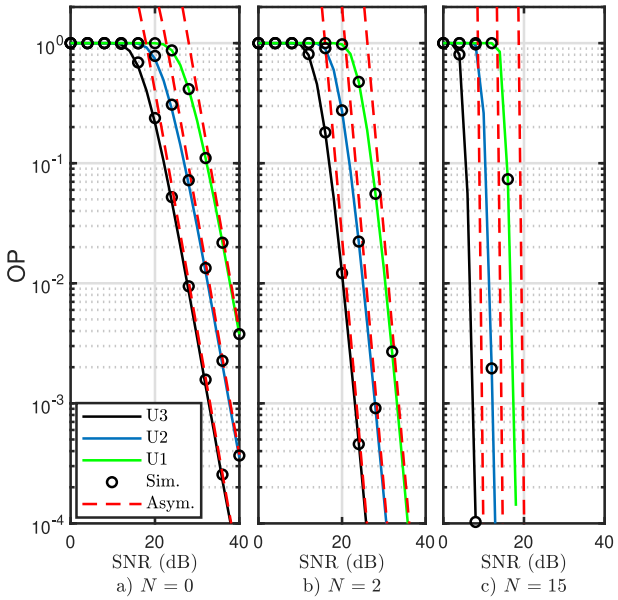

FIGURE 2. OP of three users versus SNR.

IV. MOS-BASED QOE EVALUATION MODEL FOR WEB BROWSING

MOS is normally employed to measure the user's QoE for services such as Web browsing, video streaming, and file download. In this work, we concentrate on Web browsing applications as it is one of the most widely used applications in wireless networks. MOS delineates the subjective human awareness of quality for the purpose of Web browsing applications to the objective metrics. According to [37], the appropriate model that described MOS for Web browsing applications is defined as:

$$\mathrm{MOS}_{web} = -\xi_1\ln(d(\mathrm{R}_i) + \xi_2, \tag{52}$$

$$\bar{C}_1 = \frac{\mathrm{BW}}{\ln(2)}\mathcal{D}_1\Upsilon_1 \times \left(\mathrm{G}_{3,2}^{1,3}\left[\left(\frac{N\mu(1+\kappa)}{\bar{\gamma}_1}\right)^{-1}\middle|\begin{matrix}1,1,1-(c+N\mu)\\1,0\end{matrix}\right] - \mathrm{G}_{3,2}^{1,3}\left[\Psi\left(\frac{N\mu(1+\kappa)}{\bar{\gamma}_1}\right)^{-1}\middle|\begin{matrix}1,1,1-(c+N\mu)\\1,0\end{matrix}\right]\right) \tag{47}$$

$$\bar{C}_2 = \frac{\mathrm{BW}}{\ln(2)}\mathcal{D}_2\Upsilon_2 \times \left(\mathrm{G}_{3,2}^{1,3}\left[\Psi\left(\frac{N\mu(1+\kappa)}{\bar{\gamma}_2}\right)^{-1}\middle|\begin{matrix}1,1,1-(c+N\mu)\\1,0\end{matrix}\right] - \mathrm{G}_{3,2}^{1,3}\left[a_3\left(\frac{N\mu(1+\kappa)}{\bar{\gamma}_2}\right)^{-1}\middle|\begin{matrix}1,1,1-(c+N\mu)\\1,0\end{matrix}\right]\right) \tag{48}$$

$$\bar{C}_3 = \frac{\mathrm{BW}}{\ln(2)}\mathcal{D}_3\Upsilon_3 \times \left(\mathrm{G}_{3,2}^{1,3}\left[a_3\left(\frac{N\mu(1+\kappa)}{\bar{\gamma}_3}\right)^{-1}\middle|\begin{matrix}1,1,1-(c+N\mu)\\1,0\end{matrix}\right]\right) \tag{49}$$

where ξ_1 and ξ_2 are obtained by analyzing the experimental results of Web browsing, which are constant and set to become 1.120 and 4.6746, respectively, as in [38]. $d(\mathrm{R}_i)$ indicates the delay time that is consumed between a request, made by a user, for a Web page and the display of the Web contents. It mainly relies on different components such as the Web page size, known as the round trip time (RTT), and the effects of the applied transfer of data protocols. Hence, we consider Hypertext Transfer Protocol (HTTP) and Transmission Control Protocol (TCP) in this work. Therefore, $d(\mathrm{R}_i)$ can be given accordingly to [38] as follows.

$$d(\mathrm{R}_i) = 3\mathrm{RTT} + \frac{\mathrm{FS}}{\mathrm{R}_i} + \mathcal{L}\left(\frac{\mathrm{MSS}}{\mathrm{R}_i} + \mathrm{RTT}\right) - \frac{2\mathrm{MSS}\left(2^{\mathcal{L}} - 1\right)}{\mathrm{R}_i} \tag{53}$$

where RTT stands for the round trip time in seconds, MSS defines the maximum segment size in bits, and FS is the Web page size in bits. However, the number of slow begin cycles with idle duration can be represented by $\mathcal{L} = \min\{\mathcal{L}_1, \mathcal{L}_2\}$, where $\mathcal{L}_1$ indicates the number of cycles required for the congestion window to achieve the bandwidth-delay product and $\mathcal{L}_2$ represents the amount of slow begin cycles required until the entire Web page size is successfully transmitted. Both factors can be given as follows.

$$\mathcal{L}_1 = \log_2\left(\frac{\mathrm{R}_i \times \mathrm{RTT}}{\mathrm{MSS}} + 1\right) - 1 \tag{54}$$

$$\mathcal{L}_2 = \log_2\left(\frac{\mathrm{FS}}{2 \times \mathrm{MSS}} + 1\right) - 1. \tag{55}$$

According to [24], RTT has an insignificant impact on MOS compared to the other factors of data rate, Web page, etc. In addition, RTT is expected to drop to less than 10 ms in 5G and beyond, therefore, RTT $\approx 0ms$ is assumed. As a consequence, (53) can be rewritten accordingly to $d(\mathrm{R}_i) = \frac{\mathrm{FS}}{\mathrm{R}_i}$. Thus, the MOS function of each assigned user can be expressed as follows.

$$\mathrm{MOS}_{web} = \xi_1 \ln(d(\mathrm{R}_i)) + \Lambda, \tag{56}$$

where $\Lambda = \xi_2 + \xi_1 \ln(\frac{\mathrm{BW}}{\mathrm{FS}})$.

V. NUMERICAL RESULTS

In this part, various graphs of numerical and Monte Carlo simulation results are presented to validate the derived closed-form expressions and provide some insight into the performance of the system under consideration. The main simulation parameters, applied to this work, are listed in Table 3. Furthermore, the channel is classified as quasi-static, as in it remains constant for the period of one symbol but varies randomly across successive symbol intervals. The simulation processes 10^6 symbols in each run.

Fig. 2 illustrates the OP versus SNR for three NOMA users for different numbers of passive reflectors. It can be seen that the IRS has a significant impact on outage performance of all the users. Therefore, as the number of passive reflectors N on the IRS increases, the OP of all users decreases. For example, an improvement of about 20 dB is gained for U_3 to achieve 10^{-3} of OP when N increases to 15.

TABLE 3. Simulation parameters.

Parameter	Value
Transmitted SNR (ρ)	(0-40) dB
Carrier Frequency (f)	900 MHz
Noise power (σ)	-174 dBm
Power allocation factors (a_1, a_2, a_3)	(0.75, 0.2, 0.05)
Indoor distance (d_{in})	2 m
Internal walls (n)	1
External distance (d_{rb_i})	(700,450,100) m
perpendicular loss (L_{pc})	7 dB
Parallel penetration loss (L_{pt})	20 dB

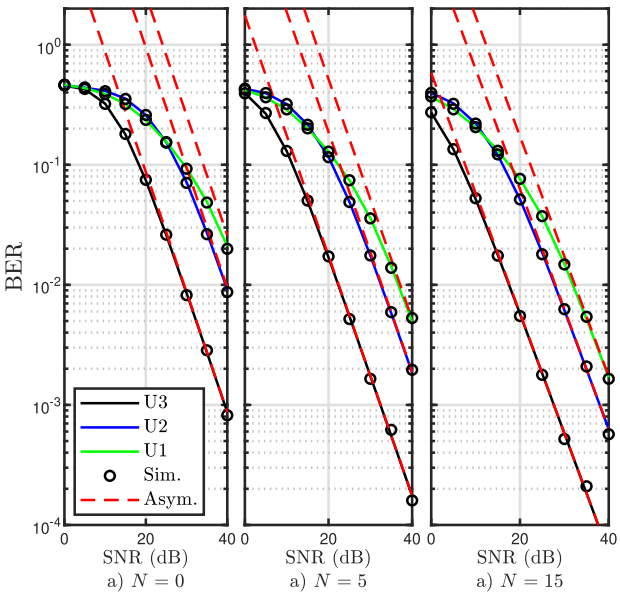

FIGURE 3. BER of three users versus SNR.

Fig. 3 shows the BER performance versus SNR for the three users considering the exist and the absence of IRS reflectors, that is $N = \{1, 5, 15\}$. As can be seen from this figure that increasing the number of IRS reflectors can lead to reducing the BER. For example, when $N = 1$, U_1 requires more than 40 dB to reach 10^{-2} of the target BER, however, if N increases by 15, then U_1 needs approximately 25 dB less to achieve the similar BER target. This analysis can be repeated to all remaining users over different aspect of BER targets. Furthermore, this figure shows the performance of BER at high average SNR, where an accurate match of the exact and asymptotic curves is achieved at high SNR.

Fig. 4 demonstrates the significant improvement in total throughput for each user when considering a different number of N reflectors. It can be observed that a low SNR is required to meet the predefined data rate for each user at

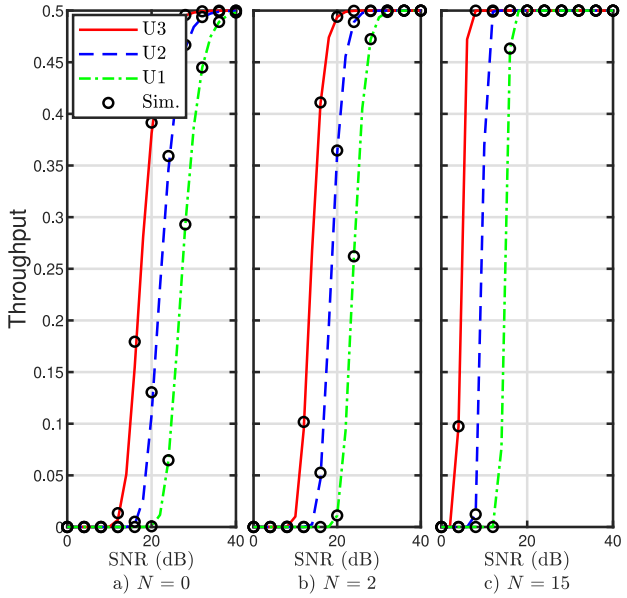

FIGURE 4. Performance of three users throughput versus SNR, $R_1 = 0.5$, $R_2 = 1$, $R_3 = 2$.

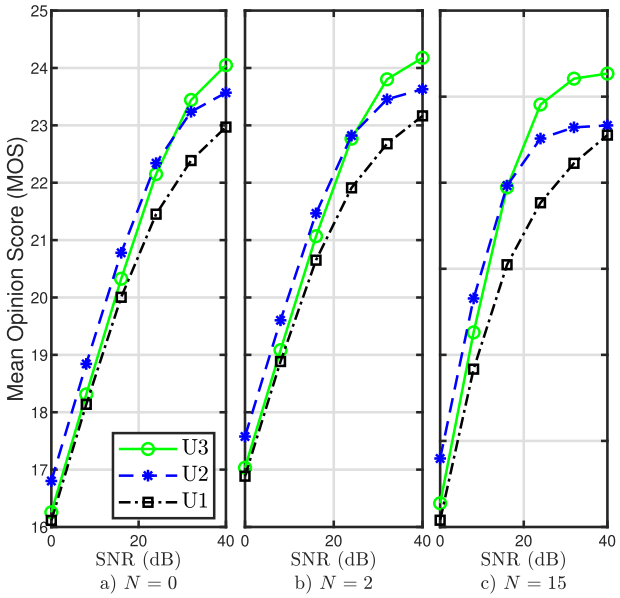

FIGURE 6. Mean opinion score (MOS) of three users versus SNR.

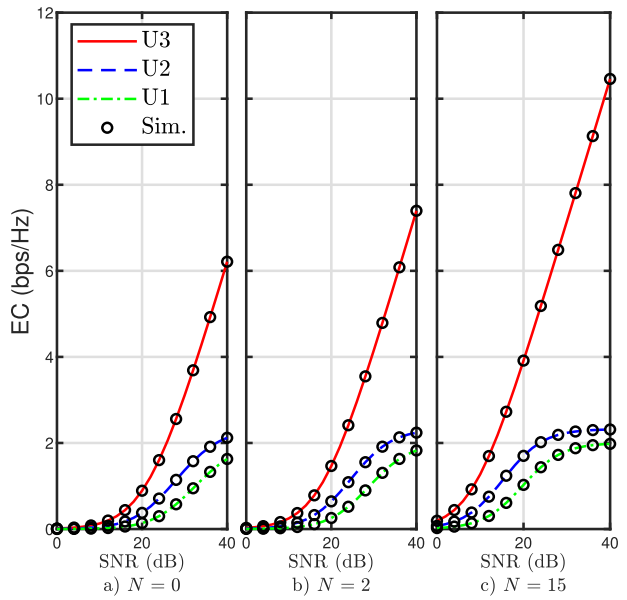

FIGURE 5. Ergodic capacity (EC) of three users versus SNR.

high values of N. For instance, in Fig. 4b, U_3 requires about 15 dB less than in the case of $N = 2$ to satisfy its target data rate. It further confirms the advantages of applying more passive reflectors in IRS.

Fig. 5 shows the ergodic capacity (EC) of three indoor NOMA users versus their transmitted SNR in dB. As it is expected that U_3 has the potential amount of capacity compared with the other users in all scenarios of N values due to its channel privileges. However, U_1, which suffers more than others, can be improved by increasing the number of N reflectors. For example, in the worst case of SNR, i.e., when SNR is less than 20 dB, U_1's capacity is dramatically increased when $N = 15$.

On the other hand, Fig. 6 presents the MOS of each user with different values of N, where MOS measures QoE. In the case of $N = 2$, it is observed that the MOS of U_3 overlaps with U_2 at about 22 dB and with U_1 at very low SNR. However, a critical overlap point is sketched at about 18 dB between both users in Fig. 6b, where $N = 15$. This is due to the different impacts caused by different factors, such as amount of IRS reflectors, channel gains, power allocation coefficients, intra-cell interference, distance from the BS, etc. Hence, manipulating these factors can lead to different outcomes for MOS. Furthermore, noticeable improvements in MOS can be gained by increasing the total number of IRS passive reflectors.

Fig. 7 shows the sum MOS of all users versus the Web page size within certain value of 10 dB SNR and different numbers of N. The results show that a large improvement of MOS can be achieved with a low Web page size, however, the larger the size of the Web page, the lower the MOS. Moreover, increasing the number of N reflectors in the IRS improves the sum MOS. Furthermore, the key difference in the sum improvement of MOS gained by low N is approximately 8 times the enhancement obtained at high N. The reason behind this behavior is related to the same impact factors mentioned in the previous figure.

VI. CONCLUSION

This paper considered the QoS and QoE of IRS-assisted indoor NOMA systems in $\kappa-\mu$ fading channels. Specifically, we studied the OP, EC, BER, throughput, and the MOS-based QoE of the considered system model. The accuracy of the derived closed-form expressions was corroborated by Monte Carlo simulations. The results demonstrate the impact of

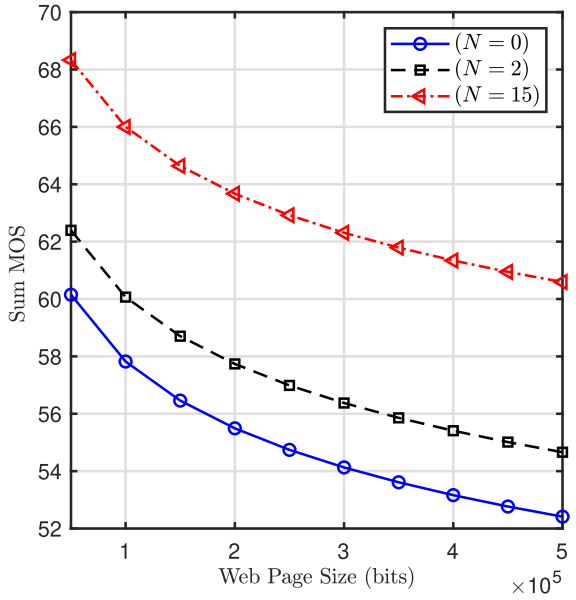

FIGURE 7. Sum mean opinion score (MOS) of three users versus Web page size, SNR=10 dB.

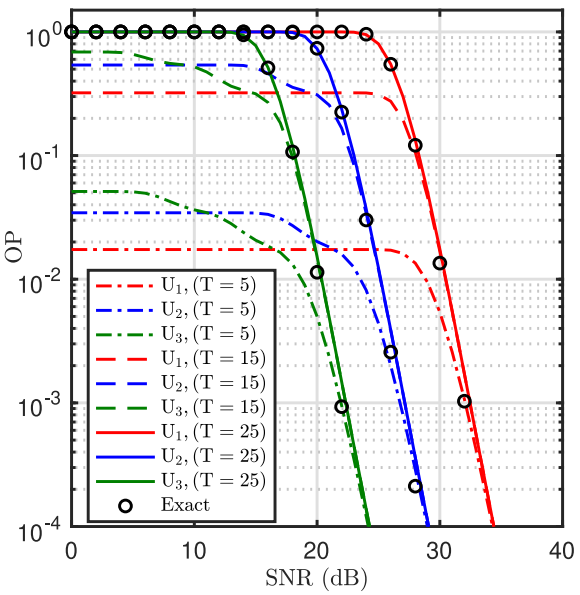

FIGURE 8. Series approximation for the OP considering less sever fading, i.e., $\kappa = 4.5$, $\mu = 4.5$. The figure presents the performance of the series approximation proposed in (16) for the OP of multiple NOMA users.

IRS, particularly as we increase the number of reflectors, on enhancing the overall user experience and service, as well as improving the MOS in the case of small Web page sizes. Furthermore, the presented results provide an insight into the system's performance with respect to various important factors, such as the fading components κ and μ, the power allocation factors, the predefined data rates, the distance from the BS and the components of indoor environments.

Future directions of this work may focus on analysing and optimizing other realistic model that involve different challenges such as multiple transmitting and receiving antennas, multiple NOMA users, imperfect SIC, practical CSI, and phase estimation errors. In addition to that, studying more performance metrics of both QoS and QoE under different channel fading and deployments of IRS-NOMA configurations could also be of interest to the community.

LIST OF ACRONYMS

5G	fifth generation
6G	Sixth generation
AWGN	additive white Gaussian noise
BER	bit error rate
BS	base station
BW	system bandwidth
CDF	cumulative distribution function
CDMA	code-division multiple access
CSI	channel state information
EC	ergodic capacity
HTTP	hypertext Transfer Protocol
i.i.d.	independent and identically distributed
IRS	intelligent reflecting surfaces
LOS	line of sight
MISO	multiple input single output
MOS	mean score opinion
MSS	maximum segment size
NLOS	non-line of sight
NOMA	non-orthogonal multiple accesses
OMA	orthogonal multiple access
OP	outage probability
PDF	probability density function
QAM	quadrature amplitude phase
QoE	quality of experience
QoS	quality of service
RTT	round trip time
RV	random variables
SC	superposition coding
SIC	successive interference cancellation
SINR	signal to interference plus noise ratio
SNR	signal-to-noise ratio
TCP	transmission Control Protocol
WPT	wireless power transfer

REFERENCES

[1] L. Dai, B. Wang, Y. Yuan, S. Han, I. Chih-lin, and Z. Wang, "Non-orthogonal multiple access for 5G: Solutions, challenges, opportunities, and future research trends," *IEEE Commun. Mag.*, vol. 53, no. 9, pp. 74–81, Sep. 2015.

[2] Z. Ding and H. V. Poor, "A simple design of IRS-NOMA transmission," *IEEE Commun. Lett.*, vol. 24, no. 5, pp. 1119–1123, May 2020.

[3] B. Makki, K. Chitti, A. Behravan, and M.-S. Alouini, "A survey of NOMA: Current status and open research challenges," *IEEE Open J. Commun. Soc.*, vol. 1, pp. 179–189, 2020.

[4] M. Z. Chowdhury, M. Shahjalal, S. Ahmed, and Y. M. Jang, "6G wireless communication systems: Applications, requirements, technologies, challenges, and research directions," *IEEE Open J. Commun. Soc.*, vol. 1, pp. 957–975, 2020.

[5] C. Huang, A. Zappone, G. C. Alexandropoulos, M. Debbah, and C. Yuen, "Reconfigurable intelligent surfaces for energy efficiency in wireless communication," *IEEE Trans. Wireless Commun.*, vol. 18, no. 8, pp. 4157–4170, Aug. 2019.

[6] Z. Ding, X. Lei, G. K. Karagiannidis, R. Schober, J. Yuan, and V. K. Bhargava, "A survey on non-orthogonal multiple access for 5G networks: Research challenges and future trends," *IEEE J. Sel. Areas Commun.*, vol. 35, no. 10, pp. 2181–2195, Oct. 2017.
[7] Z. Ding, Z. Yang, P. Fan, and H. V. Poor, "On the performance of non-orthogonal multiple access in 5G systems with randomly deployed users," *IEEE Signal Process. Lett.*, vol. 21, no. 12, pp. 1501–1505, Dec. 2014.
[8] M. Fu, Y. Zhou, and Y. Shi, "Intelligent reflecting surface for downlink non-orthogonal multiple access networks," in *Proc. IEEE Globecom Workshops (GC Wkshps)*, 2019, pp. 1–6.
[9] B. K. S. Lima et al., "Aerial intelligent reflecting surfaces in MIMO-NOMA networks: Fundamentals, potential achievements, and challenges," *IEEE Open J. Commun. Soc.*, vol. 3, pp. 1007–1024, 2022.
[10] Z. Ding et al., "A state-of-the-art survey on reconfigurable intelligent surface-assisted non-orthogonal multiple access networks," *Proc. IEEE*, vol. 110, no. 9, pp. 1358–1379, Sep. 2022.
[11] B. Zheng, Q. Wu, and R. Zhang, "Intelligent reflecting surface-assisted multiple access with user pairing: NOMA or OMA?" *IEEE Commun. Lett.*, vol. 24, no. 4, pp. 753–757, Apr. 2020.
[12] F. E. Bouanani, S. Muhaidat, P. C. Sofotasios, O. A. Dobre, and O. S. Badarneh, "Performance analysis of intelligent reflecting surface aided wireless networks with wireless power transfer," *IEEE Commun. Lett.*, vol. 25, no. 3, pp. 793–797, Mar. 2021.
[13] M. Al-Jarrah, E. Alsusa, A. Al-Dweik, and D. K. C. So, "Capacity analysis of IRS-based UAV communications with imperfect phase compensation," *IEEE Wireless Commun. Lett.*, vol. 10, no. 7, pp. 1479–1483, Jul. 2021.
[14] M. Al-Jarrah, A. Al-Dweik, E. Alsusa, Y. Iraqi, and M.-S. Alouini, "On the performance of IRS-assisted multi-layer UAV communications with imperfect phase compensation," *IEEE Trans. Commun.*, vol. 69, no. 12, pp. 8551–8568, Dec. 2021.
[15] Z. Ding, R. Schober, and H. V. Poor, "On the impact of phase shifting designs on IRS-NOMA," *IEEE Commun. Lett.*, vol. 9, no. 10, pp. 1596–1600, Oct. 2020.
[16] T. Hou, Y. Liu, Z. Song, X. Sun, Y. Chen, and L. Hanzo, "Reconfigurable intelligent surface aided NOMA networks," *IEEE J. Sel. Areas Commun.*, vol. 38, no. 11, pp. 2575–2588, Nov. 2020.
[17] J. Zhu, Y. Huang, J. Wang, K. Navaie, and Z. Ding, "Power efficient IRS-assisted NOMA," *IEEE Trans. Commun.*, vol. 69, no. 2, pp. 900–913, Feb. 2021.
[18] F. Fang, Y. Xu, Q.-V. Pham, and Z. Ding, "Energy-efficient design of IRS-NOMA networks," *IEEE Trans. Veh. Technol.*, vol. 69, no. 11, pp. 14088–14092, Nov. 2020.
[19] H. Yahya, E. Alsusa, and A. Al-Dweik, "Exact BER analysis of NOMA with arbitrary number of users and modulation orders," *IEEE Trans. Commun.*, vol. 69, no. 9, pp. 6330–6344, Sep. 2021.
[20] B. M. ElHalawany, F. Jameel, D. B. da Costa, U. S. Dias, and K. Wu, "Performance analysis of downlink NOMA systems over κ-μ shadowed fading channels," *IEEE Trans. Veh. Technol.*, vol. 69, no. 1, pp. 1046–1050, Jan. 2020.
[21] A. Alqahtani, E. Alsusa, A. Al-Dweik, and M. Al-Jarrah, "Performance analysis for downlink NOMA over α-μ generalized fading channels," *IEEE Trans. Veh. Technol.*, vol. 70, no. 7, pp. 6814–6825, Jul. 2021.
[22] H. Shao, H. Zhao, Y. Sun, J. Zhang, and Y. Xu, "QoE-aware downlink user-cell association in small cell networks: A transfer-matching game theoretic solution with peer effects," *IEEE Access*, vol. 4, pp. 10029–10041, 2016.
[23] Y. Sun, H. Shao, Z. Du, and J. Cai, "QoE-oriented resource allocation for downlink non-orthogonal multiple access," *IEEE Commun. Lett.*, vol. 25, no. 7, pp. 2362–2365, Jul. 2021.
[24] J. Cui, Y. Liu, Z. Ding, P. Fan, and A. Nallanathan, "QoE-based resource allocation for multi-cell NOMA networks," *IEEE Trans. Wireless Commun.*, vol. 17, no. 9, pp. 6160–6176, Sep. 2018.
[25] E. Basar, M. D. Renzo, J. De Rosny, M. Debbah, M.-S. Alouini, and R. Zhang, "Wireless communications through reconfigurable intelligent surfaces," *IEEE Access*, vol. 7, pp. 116753–116773, 2019.
[26] E. Basar, "Transmission through large intelligent surfaces: A new frontier in wireless communications," in *Proc. Eur. Conf. Netw. Commun. (EuCNC)*, 2019, pp. 112–117.
[27] Y. Cheng, K. H. Li, Y. Liu, K. C. Teh, and H. V. Poor, "Downlink and uplink intelligent reflecting surface aided networks: NOMA and OMA," *IEEE Trans. Wireless Commun.*, vol. 20, no. 6, pp. 3988–4000, Jun. 2021.
[28] A. Alqahtani, E. A. Alsusa, and A. Al-Dweik. "UAV-enabled cooperative NOMA with indoor-outdoor user-paring and SWIPT in κ-μ channels." TechRxiv. 2021. [Online]. Available: https://doi.org/10.36227/techrxiv.16653094.v1
[29] M. Hamza and M. Hadzialic, "BEP/SEP and outage performance analysis of L-branch maximal-ratio combiner for $\kappa - \mu$ fading," *Int. J. Digit. Multimedia Broadcast.*, vol. 2009, pp. 1–8, Jan. 2019.
[30] A. Jeffrey and D. Zwillinger, *Table of Integrals, Series, and Products*, 7th ed. Waltham, MA, USA: Academic, 2007.
[31] A. Prudnikov, Y. Brychkov, and O. Marichev, *Integrals and Series. More Special Functions*, vol. 3. London, U.K.: Godron Breach Sci., 1990.
[32] M. Springer and K. M. R. Collection, *The Algebra of Random Variables*. New York, NY, USA: Wiley, 1979.
[33] A. A. Kilbas and M. Saigo, "On the H-function," *J. Appl. Math. Stoch. Anal.*, vol. 12, no. 2, pp. 191–204, 1999.
[34] M. K. Simon and M.-S. Alouini, *Digital Communication Over Fading Channels*, 2nd ed. New York, NY, USA: Wiley, 2004.
[35] A. Mathai, R. Saxena, and H. Haubold, *The H-Function: Theory and Applications*. New York, NY, USA: Springer, 2009.
[36] K. Peppas, F. Lazarakis, A. Alexandridis, and K. Dangakis, "Simple, accurate formula for the average bit error probability of multiple-input multiple-output free-space optical links over negative exponential turbulence channels," *Opt. Lett.*, vol. 37, pp. 3243–3245, Aug. 2012.
[37] M. Rugelj, U. Sedlar, M. Volk, J. Sterle, M. Hajdinjak, and A. Kos, "Novel cross-layer QoE-aware radio resource allocation algorithms in multiuser OFDMA systems," *IEEE Trans. Commun.*, vol. 62, no. 9, pp. 3196–3208, Sep. 2014.
[38] P. Ameigeiras, J. J. Ramos-Munoz, J. Navarro-Ortiz, P. Mogensen, and J. M. Lopez-Soler, "QoE oriented cross-layer design of a resource allocation algorithm in beyond 3G systems," *Comput. Commun.*, vol. 33, no. 5, pp. 571–582, 2010.

ADEL ALQAHTANI (Member, IEEE) received the Ph.D. degree in electrical and electronic engineering from the University of Manchester, U.K., in 2022, and the M.Sc. degree in telecommunications from George Mason University, USA, in 2017. He is currently an Assistant Professor with the Department of Electrical Engineering, King Khalid University, Saudi Arabia. His research interests include 5G, 6G and beyond wireless communication networks, NOMA technology, cooperative relay networks, resource allocation optimization, and re-configurable intelligent surfaces.

EMAD ALSUSA (Senior Member, IEEE) is the Head of the Communication and RF Research Group with the Department of Electrical and Electronic Engineering, University of Manchester. His research interest is in the area of wireless networks and signal processing with particular focus on future ultra-efficient networks through the design of novel techniques for radio resource management, interference manipulation, secrete key exchange, and energy neutrality. He has received a number of awards, including the Best Paper Awards in the IEEE international Symposium on Power Line Communications in 2014, the IEEE Wireless Communications and Networking Conference in 2019, the IEEE International Symposium on Networks, and the Computers and Communications (ISNCC'21). He served as a Conference General Co/Chair of the IEEE OnlineGreencom in 2017 and Sustainability through ICT Summit in 2019, as well as the TPC Symposia-Co/Chair in several IEEE conferences, including VTC'16, GISN'16, PIMRC'17, Globecom'18, and Globecom'23. He is a U.K. representative in the International Union of Radio Science.